Incompressible Stokes flow in an annulus: An analytical solution and numerical benchmark

C. Thieulot[a,*], E.G. Puckett[b]

[a] *Department of Earth Sciences, Utrecht University, The Netherlands*
[b] *Department of Mathematics, U.C. Davis, Davis, CA 95616, USA*

Abstract

We present a new family of analytical solutions to the incompressible Stokes equation in an annulus with a constant viscosity, a gravity field that points towards the center of the annulus, and a density field that depends on the spatial coordinates. The velocity is tangential to both the inner and the outer boundaries and is such that it produces convection cells, the number of which is parametrized by a single parameter k . This benchmark has been implemented in the finite element geodynamics codes ASPECT and ELEFANT. We report convergence rates for the velocity and pressure as well as global velocity averages.

Keywords: Finite Element Method; Incompressible Stokes equations; Incompressible Stokes flow in an annulus; Benchmark for Stokes flow in an annulus;

[1]

*Corresponding Author
Email address: `c.thieulot@uu.nl` (C. Thieulot)

[1] Authors CT and EGP derived the analytical benchmark together. CT implemented the benchmark in both ASPECT and ELEFANT codes. CT and EGP wrote the manuscript together.

1. Introduction

Numerical modeling is a essential component of our understanding of convection in the Earth's mantle [1] as it allows geodynamicists to test hypotheses and build ever more refined models of mantellic processes. Given the vastly different time scales of the dynamics of the core from that of the mantle and the vast differences between the rheologies of these two regions, rather than using computer models in spheres researchers have developed two dimensional models of the Earth's mantle in annuli [2, 3, 4, 5, 6, 7, 8, 9] and three dimensional models in spherical shells [10, 11, 12, 13, 14, 15, 16].

While there are only a few analytical and numerical benchmarks in 3D spherical shells [12, 14, 17] there a great many on rectangular grids in rectangular, two-dimensional Cartesian domains [18, 19, 20, 21, 22]. However, to our knowledge, there are no non-trivial, incompressible, isoviscous, and isothermal benchmarks that involve an exact solution of the incompressible Stokes equations in a two-dimensional annulus.

We have developed such a benchmark for an isoviscous, isothermal solution of the incompressible Stokes equations for which simple kinematic boundary conditions lead to structures that are serve as a model of "convection cells", where the number of these cells is determined by a single parameter k. These cells are kinematic, isothermal counterparts of those found in full mantle convection experiments and computations.

In Section 2 we present the derivation of our analytical solution to the isoviscous, isothermal incompressible Stokes equations in an annulus and in Section 3 we compare our numerical computations of these solutions with the exact analytical solution.

2. Derivation of the Exact Solution

We seek an exact solution to the incompressible Stokes equations for an isoviscous, isothermal fluid in an annulus. Given the geometry of the problem, we work in polar coordinates. We denote the orthonormal basis vectors by $\mathbf{e}_r$ and $\mathbf{e}_\theta$, the inner radius of the annulus by R_1 and the outer radius by R_2. Further, we assume that the viscosity μ is constant, which we set to $\mu = 1$ we set the gravity vector to $\mathbf{g} = -g_r\,\mathbf{e}_r$ with $g_r = 1$.

Given these assumptions, the incompressible Stokes equations in the annulus are [23]

$$\frac{\partial^2 v_r}{\partial r^2} + \frac{1}{r}\frac{\partial v_r}{\partial r} + \frac{1}{r^2}\frac{\partial^2 v_r}{\partial \theta^2} - \frac{v_r}{r^2} - \frac{2}{r^2}\frac{\partial u_\theta}{\partial \theta} - \frac{\partial p}{\partial r} - \rho g_r \quad = \quad 0 \tag{1}$$

$$\frac{\partial^2 v_\theta}{\partial r^2} + \frac{1}{r}\frac{\partial v_\theta}{\partial r} + \frac{1}{r^2}\frac{\partial^2 v_\theta}{\partial \theta^2} + \frac{2}{r^2}\frac{\partial v_r}{\partial \theta} - \frac{v_\theta}{r^2} - \frac{1}{r}\frac{\partial p}{\partial \theta} \quad = \quad 0 \tag{2}$$

$$\frac{1}{r}\frac{\partial (r v_r)}{\partial r} + \frac{1}{r}\frac{\partial v_\theta}{\partial \theta} \quad = \quad 0 \tag{3}$$

Equations (1) and (2) are the momentum equations in polar coordinates while Equation (3) is the incompressibility constraint.

We now postulate the θ-component of velocity vector can be written as

$$v_\theta(r,\theta) = f(r)\cos(k\theta) \tag{4}$$

where the function $f(r)$ will be specified later. From Equation (3) we can write

$$\frac{\partial(rv_r)}{\partial r} = -\frac{\partial v_\theta}{\partial \theta} = kf(r)\sin(k\theta) \tag{5}$$

leading to

$$v_r(r,\theta) = g(r)k\sin(k\theta) \tag{6}$$

where

$$g(r) = \frac{1}{r}\int f(r)dr \tag{7}$$

Since the velocity is tangential to both boundaries we have

$$v_r(r=R_1,\theta) = v_r(r=R_2,\theta) = 0 \tag{8}$$

for all $\theta \in [0,2\pi]$. By taking $f(r) = Ar + B/r$, (e.g., see the solution of the Laplace equation in an annulus in [24] for $n = 0$, 1) one obtains

$$g(r) = \frac{A}{2}r + \frac{B}{r}\ln r + \frac{C}{r} \tag{9}$$

where C is a non-zero constant of integration. Given the boundary conditions in Equation (8) we find that

$$A = -C\frac{2(\ln R_1 - \ln R_2)}{R_2^2\ln R_1 - R_1^2\ln R_2} \tag{10}$$

$$B = -C\frac{R_2^2 - R_1^2}{R_2^2\ln R_1 - R_1^2\ln R_2} \tag{11}$$

Thus,

$$\frac{\partial^2 f}{\partial r^2} + \frac{1}{r}\frac{\partial f}{\partial r} - \frac{f}{r^2} = 0 \tag{12}$$

so that Equation (2) simplifies to

$$\frac{1}{r^2}\frac{\partial^2 v_\theta}{\partial \theta^2} + \frac{2}{r^2}\frac{\partial v_r}{\partial \theta} - \frac{1}{r}\frac{\partial p}{\partial \theta} = 0 \tag{13}$$

which leads to

$$p(r,\theta) = kh(r)\sin(k\theta) + l(r) \tag{14}$$

where $l(r)$ comes from integration with respect to θ and $h(r) = (2g(r) - f(r))/r$. We now insert Equation (14) into Equation (1) to obtain

$$\begin{aligned}\rho(r,\theta) &= \frac{\partial^2 v_r}{\partial r^2} + \frac{1}{r}\frac{\partial v_r}{\partial r} + \frac{1}{r^2}\frac{\partial^2 v_r}{\partial \theta^2} - \frac{v_r}{r^2} - \frac{2}{r^2}\frac{\partial v_\theta}{\partial \theta} - \frac{\partial p}{\partial r} \\ &= kg''(r)\sin(k\theta) + k\frac{g'(r)}{r}\sin(k\theta) - k^3\frac{g(r)}{r^2}\sin(k\theta) \\ &\quad -k\frac{g(r)}{r^2}\sin(k\theta) + k\frac{2f(r)}{r^2}\sin(k\theta) - kh'(r)\sin(k\theta) - l'(r) \\ &= \mathcal{M}(r)k\sin(k\theta) - l'(r) \end{aligned} \tag{15}$$

where

$$\mathcal{M}(r) = g'' - \frac{g'}{r} - \frac{g}{r^2}(k^2 - 1) + \frac{f}{r^2} + \frac{f'}{r}. \tag{16}$$

Taking $k = 0$ yields $\rho(r,\theta) = -l'(r)$, so we choose $l'(r) = -\rho_0$. In this case,

$$p(r,\theta)|_{k=0} = l(r) = \rho_0 g_r (R_2 - r) \tag{17}$$

where we have imposed $p(r,\theta) = 0$ at the outer radius $r = R_2$.

Equations (4), (6), and (14) are a solution of the incompressible Stokes equations. In Figure 1 we present the velocity and pressure fields for $k = 0, 1, 2$, and 4 and $\rho_0 = 0$. For $k = 0$ the velocity is tangential to both the inner and outer boundaries: it is clockwise on the inner boundary $r = R_1$ and counterclockwise on the outer boundary, $r = R_2$. thereby imposing a shear flow in the annulus. The density is purely radial as is the pressure. When $k > 0$ there are k cells or 'lobes' with positive density values and k lobes with negative values, yielding $2\,k$ convection cells.

2.1. Average Benchmark Quantities

Benchmark publications often focus on scalar quantities that represent the solution in an average sense [18, 25]. Often these quantities are velocity averages or root mean square velocities. Since we have an exact expression for the velocity field, we can compute the exact analytical value of these averages.

- θ-average of radial velocity component v_r,

$$< v_r(r) >= \frac{1}{2\pi}\int_0^{2\pi} v_r(r,\theta)d\theta = 0 \tag{18}$$

- θ-average of the velocity component v_θ,

$$< v_\theta(r) >= \frac{1}{2\pi}\int_0^{2\pi} v_\theta(r,\theta)d\theta = 0 \tag{19}$$

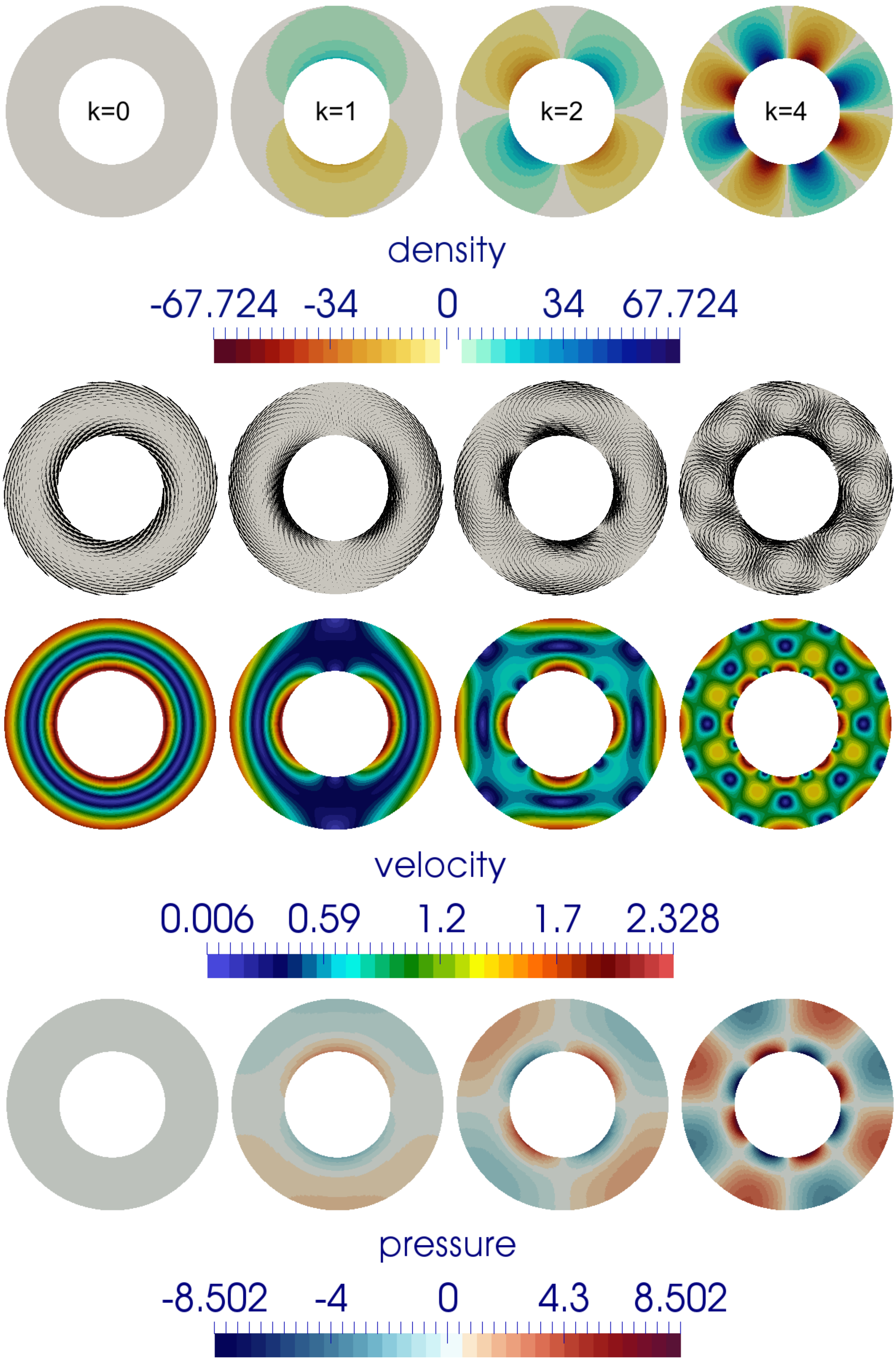

Figure 1: From left to right, increasing values of k. From top to bottom, density given by Equation (15), velocity vectors and magnitude given by Equations (4) and (6), and pressure given by Equation (14).

- θ-root mean square average of the velocity component v_r

$$< v_r(r) >_{rms} = \sqrt{\frac{1}{2\pi}\int_0^{2\pi} v_r(r,\theta)^2 d\theta} = \frac{k|g(r)|}{\sqrt{2}} \tag{20}$$

- θ-root mean square average of the velocity component v_θ

$$< v_\theta >_{rms}(r) = \sqrt{\frac{1}{2\pi}\int_0^{2\pi} v_\theta(r,\theta)^2 d\theta} = \frac{|f(r)|}{\sqrt{2}} \tag{21}$$

- Root mean square velocity v_{rms}

$$v_{rms} = \sqrt{\frac{1}{V}\int_V (v_r^2 + v_\theta^2) dV} \tag{22}$$

where V is the volume (area) of the annulus. When $k = 0$, the root mean square velocity is given by:

$$\begin{aligned} v_{rms} &= \sqrt{\frac{1}{V}\int_0^{2\pi} d\theta \int_{R_1}^{R_2} f(r)^2 r dr} \\ &= \sqrt{\frac{2}{(R_2^2 - R_1^2)}\left[\frac{A^2}{4}(R_2^4 - R_1^4) + AB(R_2^2 - R_1^2) + B^2(\ln R_2 - \ln R_1)\right]} \end{aligned} \tag{23}$$

When $k = 1$, the root mean square velocity is given by:

$$\begin{aligned} v_{rms} &= \sqrt{\frac{1}{V}\int_0^{2\pi}\int_{R_1}^{R_2} [(f(r)\cos(k\theta))^2 + (g(r)k\sin(k\theta))^2] r dr d\theta} \\ &= \left(\frac{A^2}{16}(4+k^2)(R_2^4 - R_1^4) + (\frac{AB}{4}(4-k^2) + \frac{ACk^2}{2})(R_2^2 - R_1^2)\right. \\ &+ (B^2 + C^2k^2)(\ln R_2 - \ln R_1) + BCk^2[(\ln R_2)^2 - (\ln R_1)^2] \\ &+ \left.\frac{B^2k^2}{3}[(\ln R_2)^3 - (\ln R_1)^3] + \frac{ABk^2}{2}[R_2^2 \ln R_2 - R_1^2 \ln R_1]\right)^{1/2} \\ &/ \ (R_2^2 - R_1^2)^{1/2} \end{aligned} \tag{24}$$

3. Numerical Results

The solution to the incompressible Stokes equations that we derived in Section 2 above is intended to be a numerical benchmark. In this case, the velocity is only prescribed on the inner and outer boundaries $r = R_1$, R_2 and in what follows we have set $\rho_0 = 0$.

The density is then given by Equation (15), the gravity vector is $\mathbf{g} = -\mathbf{e}_r$, and we set $C = -1$, $R_1 = 1$, and $R_2 = 2$.

We used two different computer codes to compute the following results.

- ELEFANT[2] is a FEM code [17, 26, 27] that is a successor to the FANTOM code [28], but which also has a number of improvements as compared to its predecessor. It is a finite element code that supports both triangular and quadrilateral elements. In this work we used the $Q_1 \times P_0$ element combination.

- ASPECT [3] (Advanced Solver for Problems in Earths ConvecTion) is an open source finite element code [29, 30, 31]. It is built upon deal.II [32], which is a general-purpose FEM library, TRILINOS [33], which provides scalable and parallel solvers, and p4est [34], which builds distributed, parallelized, adaptive meshes. ASPECT relies on the use of modern numerical methods, such as adaptive mesh refinement, linear and nonlinear solvers, and stabilization of transport-dominated processes. These modern methods, together with high-order elements, ensure highly accurate solutions and excellent parallel scaling that has been demonstrated for up to several thousand processors. For the benchmark problems presented in this paper we used the $Q_2 \times Q_1$ element combination in ASPECT on uniform grids. The present benchmark is implemented in ASPECT 2.0 and is referenced in the ASPECT users' manual [35].

In our computations, the finite element grids contain $n_{el} = n_r * n_t$ elements where n_r is the number of elements in the radial direction and n_t is the number of elements in the θ direction. One can check the correctness of our implementation by examining the computed pressure on the two boundaries in Figure 2, which shows both the computed and true pressures for $k = 1, 2$, and 4. One can see that there is excellent agreement between the computed values and the analytical values. The error in the computed pressure field is further documented in Figure 5.

In Figures 3 we show the computed values of the average velocities for various values of k, where the true values are from Equations (18) and (19). Note that the difference between the computed and exact values are on the order of machine precision $\mu = 10^{-16}$. In Figure 4a,b we show the computed radial and tangential root mean square velocities as compared to the true values in Equations (20) and (21). The computed and analytical profiles are indistinguishable in this Figure. We computed the root mean square velocity for various values of k and various resolutions. The values we obtained with ASPECT and ELEFANT are reported in Table 1. It is apparent that the measured values

[2] http://cedricthieulot.net/elefant.html

[3] https://aspect.geodynamics.org/

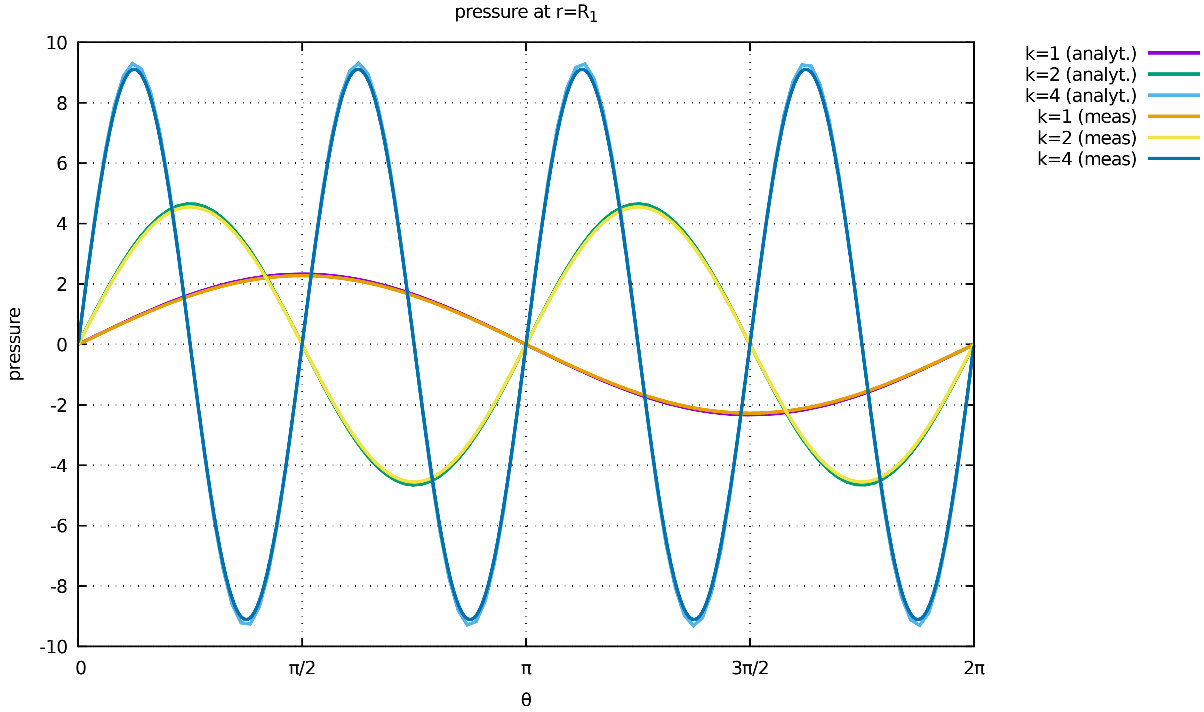

a)

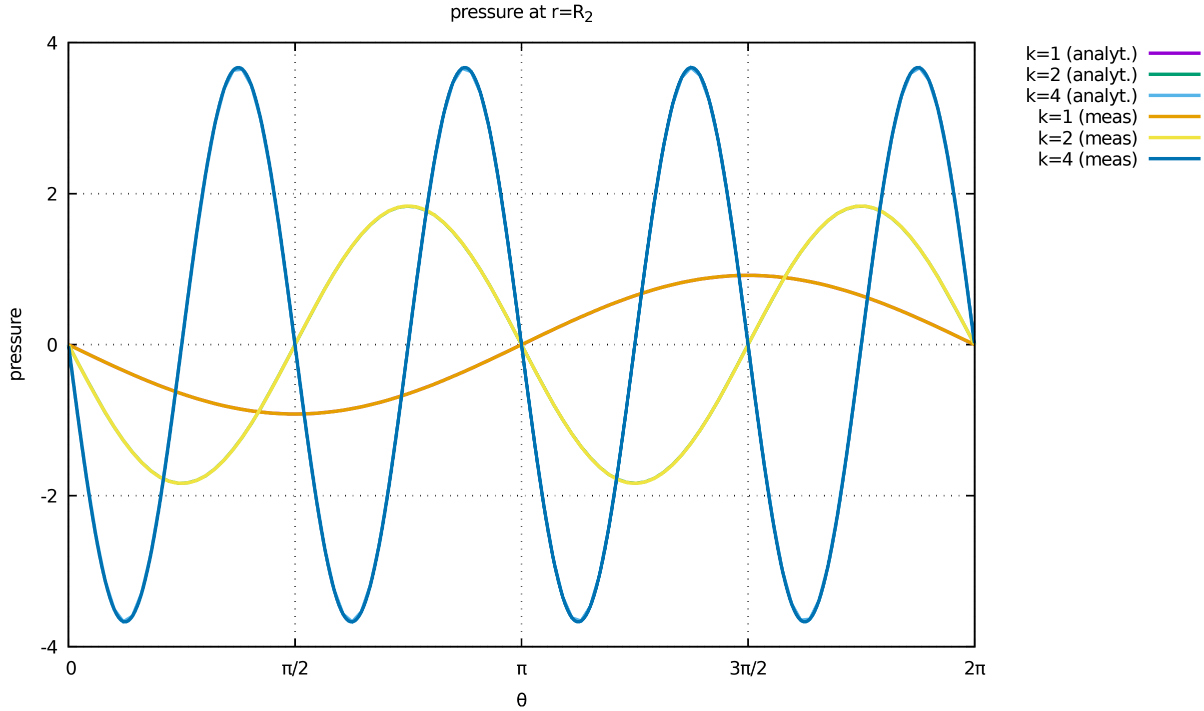

b)

Figure 2: The pressure on a) the inner boundary $r = R_1$; b) the outer boundary $r = R_2$ obtained with ELEFANT. The grid resolution is $n_r = 128$ elements in the radial direction and $n_t = 1024$ elements in the tangential direction.

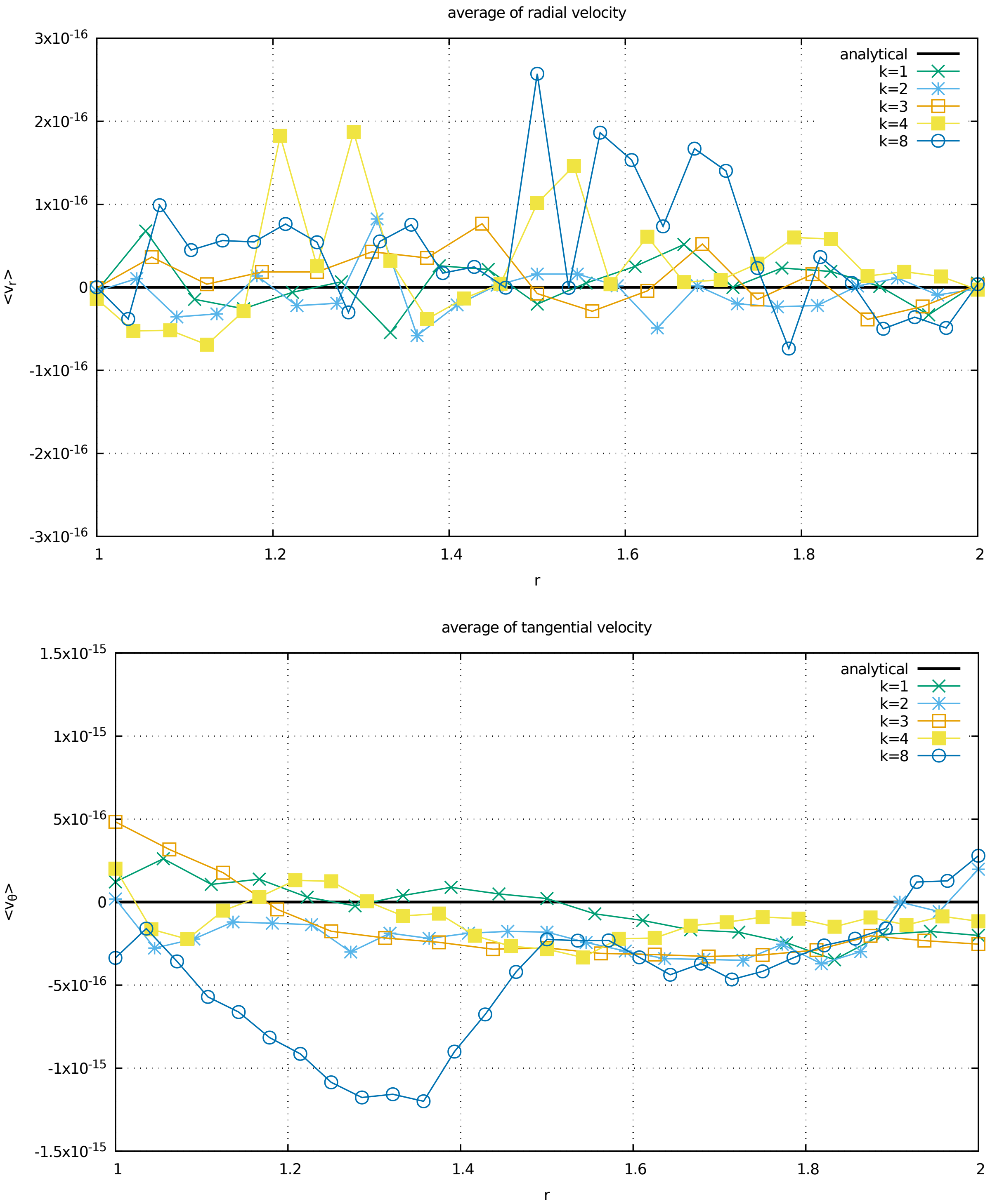

a)

b)

Figure 3: Computed radial averages of the (a) radial and (b) tangential velocity components as a function of r for $k = 1, 2, 3, 4$, and 8 versus the true values from Equations (18) and (19). Results obtained with ELEFANT.

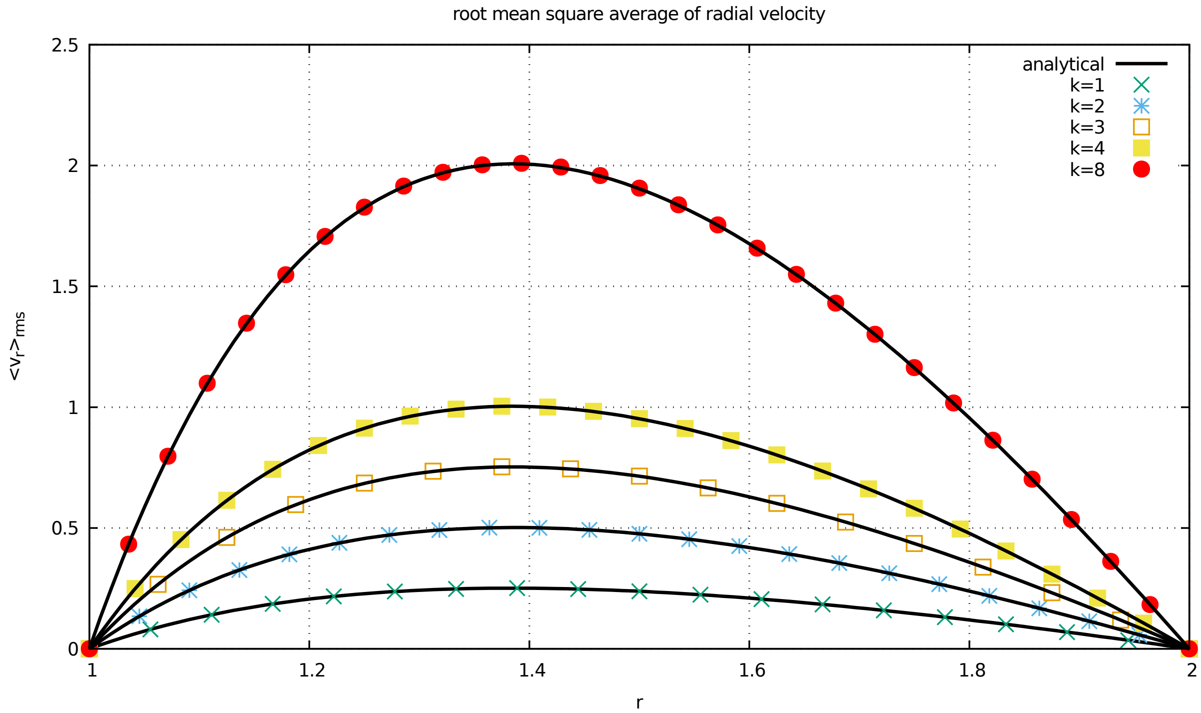

a)

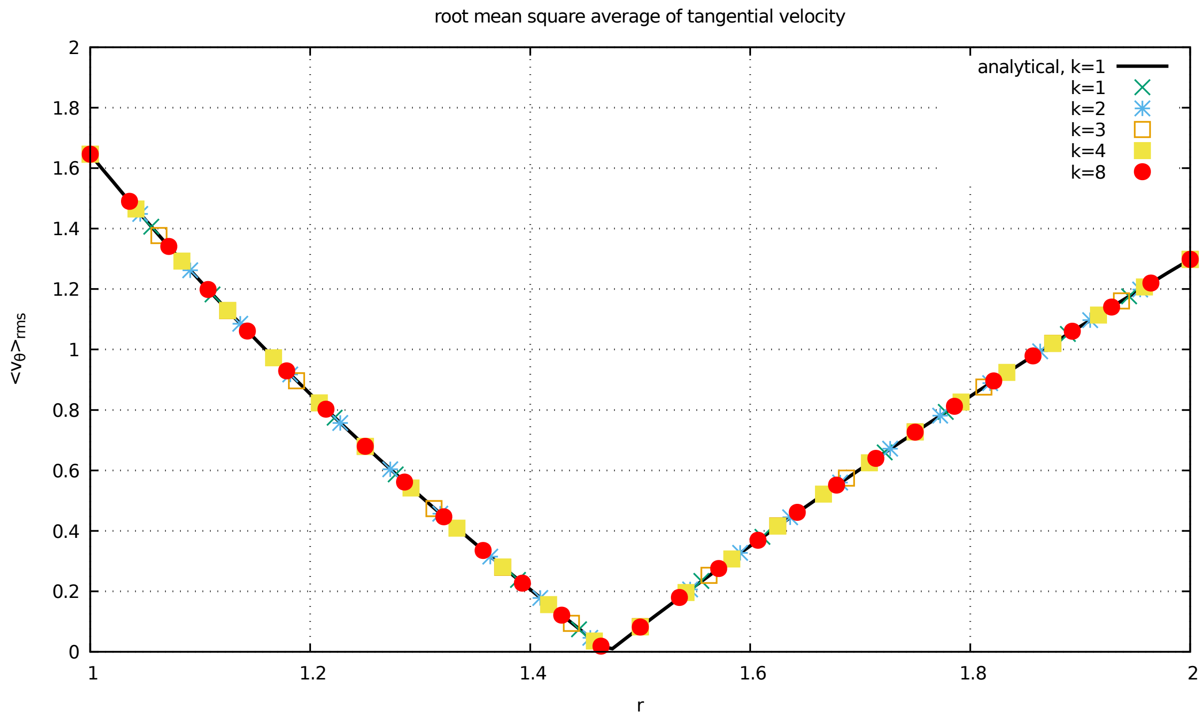

b)

Figure 4: Root mean square (a) radial and (b) tangential velocity components as a function of r for $k = 1, 2, 3, 4, 8$. Results obtained with ELEFANT. .

$n_r * n_t$	k=0	k=1	k=2	k=3	k=4	k=8
ELEFANT						
8x128	1.16053	0.83943	0.89217	0.97388	1.07810	1.61846
16x256	1.15957	0.83883	0.89280	0.97618	1.08222	1.63256
32x512	1.15932	0.83868	0.89295	0.97674	1.08322	1.63609
64x1024	1.15926	0.83864	0.89299	0.97688	1.08347	1.63697
128x2048	1.15924	0.83863	0.89300	0.97692	1.08353	1.63719
256x4096	1.15924	0.83863	0.89300	0.97693	1.08355	1.63724
ASPECT						
4×48	1.157773	0.8377398	0.89250634	0.9769904	1.0842358	1.638336
8×96	1.158835	0.8383679	0.89280005	0.9768007	1.0835105	1.637383
16×192	1.159134	0.8385620	0.89294820	0.9768854	1.0835267	1.637273
32×384	1.159211	0.8386131	0.89299078	0.9769167	1.0835465	1.637261
64×768	1.159230	0.8386260	0.8930018	0.9769253	1.0835525	1.637260
128×1536	1.159235	0.8386293	0.8930046	0.9769275	1.0835540	1.637259
Analytical	1.159236712	0.8386303476	0.8930054915	0.9769282067	1.083554613	1.637259224

Table 1: Root mean square velocity values for various values of k and grid resolutions for both ELEFANT and ASPECT.

converge to the analytical one as the mesh size $h = (R_2 - R_1)/n_r$ is decreased.

Finally, we investigate how the error in the computed solution diminishes with an increase of resolution. We then compute the L_2-norm of the error [36] for both velocity and pressure and plot these as a function of resolution and for various values of k. The resolution varied from 8×128 to 512×8192. We see that the velocity error converges like $\mathcal{O}(h^{n+1})$ while the pressure error converges like $\mathcal{O}(h^n)$ for $Q^n \times Q^{n-1}$ elements as shown in Figure 5. We also computed this test in ASPECT with $Q_2 \times P_{-1}$ elements with nearly identical results. All error measurement values are available in Appendix A.

4. Conclusions

We have derived a family of analytical solutions to the incompressible Stokes equations for an isoviscous, isothermal fluid in an annulus These solutions were implemented in two geodynamic codes, ASPECT and ELEFANT, and the accuracy of the computed solutions was checked for three finite elements combinations: $Q_1 \times P_0$, $Q_2 \times Q_1$, and $Q_3 \times Q_2$. The convergence rates were shown to be as expected from the theory of finite element methods for te incompressible Stokes equations. WE also derived several velocity field averages analytically and demonstrated that the computed values were in excellent agreement with the analytical values. Given the nature of the flow, which made up of multiple convection cells with tangential flow on the boundaries, we expect that this family of analytical solutions will become a standard benchmark for advection methods in annular geometries.

Acknowledgements

This work was supported by the US National Science Foundation (NSF) under Award number 1440811. The development of ASPECT was supported by the Computational Infrastructure for Geodynamics (CIG) under NSF Award numbers 0949446 and 1550901. The authors wish to thank the principal ASPECT developers / authors and CIG for the opportunity to initiate the collaboration between Professors Thieulot and Puckett during the third ASPECT Hackathon June 25 – July 2, 2016.

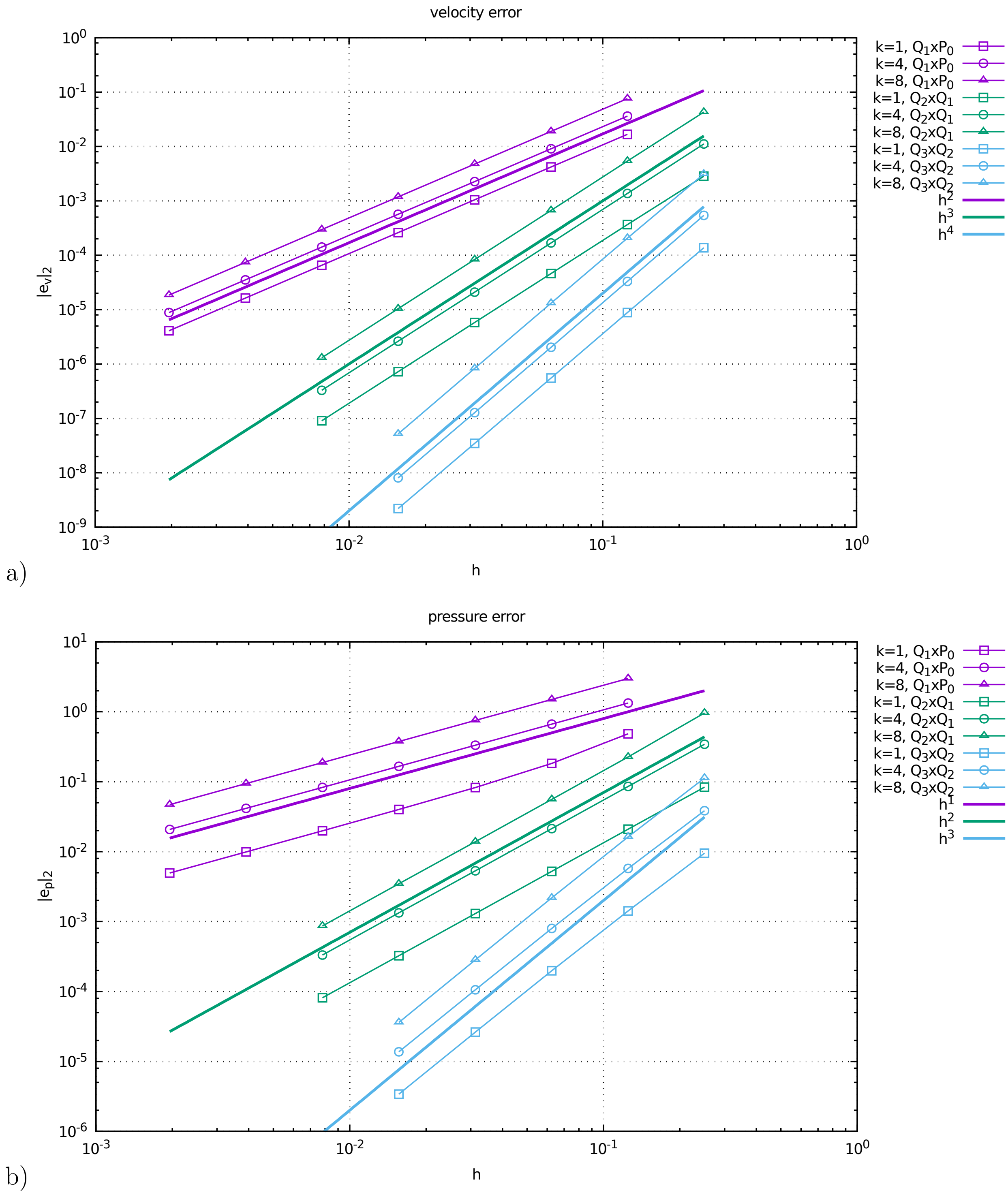

Figure 5: a) L_2-norm of the error in velocity as a function of the grid resolution h; b) L_2-norm of the error in the pressure as a function of h. ($Q_1 \times P_0$ results obtained with ELEFANT, $Q_2 \times Q_1$ and $Q_3 \times Q_2$ results obtained with ASPECT).

Appendix A. TABLES OF ERRORS

In the following tables the velocity and pressure errors of Fig. (5) are reported as well as the corresponding convergence rates which are defined as:

$$\text{rate} = \log_2 \left(\frac{err(h = 2^{n-1})}{err(h = 2^n)} \right)$$

ELEFANT ($Q_1 \times P_0$):

	$\lvert e_v\rvert_2$ ($k=1$)	rate	$\lvert e_p\rvert_2$ ($k=1$)	rate	$\lvert e_v\rvert_2$ ($k=4$)	rate	$\lvert e_p\rvert_2$ ($k=4$)	rate	$\lvert e_v\rvert_2$ ($k=8$)	rate	$\lvert e_p\rvert_2$ ($k=8$)	rate
8	1.6726×10^{-2}		4.8376×10^{-1}		3.6136×10^{-2}		$1.3340 \times 10^{+0}$		7.5685×10^{-2}		$2.9939 \times 10^{+0}$	
16	4.1829×10^{-3}	2.00	1.8261×10^{-1}	1.41	9.0391×10^{-3}	2.00	6.6485×10^{-1}	1.00	1.8932×10^{-2}	2.00	$1.5019 \times 10^{+0}$	1.00
32	1.0458×10^{-3}	2.00	8.2440×10^{-2}	1.15	2.2600×10^{-3}	2.00	3.3215×10^{-1}	1.00	4.7328×10^{-3}	2.00	7.5156×10^{-1}	1.00
64	2.6146×10^{-4}	2.00	4.0041×10^{-2}	1.04	5.6503×10^{-4}	2.00	1.6604×10^{-1}	1.00	1.1831×10^{-3}	2.00	3.7586×10^{-1}	1.00
128	6.5366×10^{-5}	2.00	1.9870×10^{-2}	1.01	1.4126×10^{-4}	2.00	8.3016×10^{-2}	1.00	2.9579×10^{-4}	2.00	1.8793×10^{-1}	1.00
256	1.6341×10^{-5}	2.00	9.9165×10^{-3}	1.00	3.5315×10^{-5}	2.00	4.1507×10^{-2}	1.00	7.3949×10^{-5}	2.00	9.3971×10^{-2}	1.00
512	4.0854×10^{-6}	2.00	4.9559×10^{-3}	1.00	8.8287×10^{-6}	2.00	2.0753×10^{-2}	1.00	1.8487×10^{-5}	2.00	4.6985×10^{-2}	1.00

ASPECT ($Q_2 \times Q_1$)

	$\lvert e_v\rvert_2$ ($k=1$)	rate	$\lvert e_p\rvert_2$ ($k=1$)	rate	$\lvert e_v\rvert_2$ ($k=4$)	rate	$\lvert e_p\rvert_2$ ($k=4$)	rate	$\lvert e_v\rvert_2$ ($k=8$)	rate	$\lvert e_p\rvert_2$ ($k=8$)	rate
4	2.8334×10^{-3}		8.3514×10^{-2}		1.1138×10^{-2}		3.4266×10^{-1}		4.2895×10^{-02}		9.6314×10^{-1}	
8	3.6567×10^{-4}	2.95	2.0923×10^{-2}	2.00	1.3661×10^{-3}	3.02	8.5717×10^{-2}	2.00	5.3779×10^{-03}	3.00	2.2629×10^{-1}	2.09
16	4.6179×10^{-5}	2.99	5.2107×10^{-3}	2.00	1.6856×10^{-4}	3.02	2.1341×10^{-2}	2.00	6.6867×10^{-04}	3.01	5.5718×10^{-2}	2.02
32	5.7907×10^{-6}	3.00	1.3001×10^{-3}	2.00	2.0998×10^{-5}	3.00	5.3248×10^{-3}	2.00	8.3418×10^{-05}	3.00	1.3874×10^{-2}	2.01
64	7.2452×10^{-7}	3.00	3.2482×10^{-4}	2.00	2.6230×10^{-6}	3.00	1.3303×10^{-3}	2.00	1.0422×10^{-05}	3.00	3.4651×10^{-3}	2.00
128	9.0590×10^{-8}	3.00	8.1192×10^{-5}	2.00	3.2786×10^{-7}	3.00	3.3254×10^{-4}	2.00	1.3028×10^{-06}	3.00	8.6605×10^{-4}	2.00

ASPECT ($Q_3 \times Q_2$)

	$\|e_v\|_2$ ($k=1$)	rate	$\|e_p\|_2$ ($k=1$)	rate	$\|e_v\|_2$ ($k=4$)	rate	$\|e_p\|_2$ ($k=4$)	rate	$\|e_v\|_2$ ($k=8$)	rate	$\|e_p\|_2$ ($k=8$)	rate
4	1.3756×10^{-4}		9.5083×10^{-3}		5.4164×10^{-4}		3.8528×10^{-2}		3.1231×10^{-3}		1.1283×10^{-1}	
8	8.8209×10^{-6}	3.96	1.4217×10^{-3}	2.74	3.2968×10^{-5}	4.04	5.7425×10^{-3}	2.75	2.0632×10^{-4}	3.92	1.6252×10^{-2}	2.80
16	5.5243×10^{-7}	4.00	1.9775×10^{-4}	2.85	2.0332×10^{-6}	4.02	7.9756×10^{-4}	2.85	1.3156×10^{-5}	3.97	2.1819×10^{-3}	2.90
32	3.4765×10^{-8}	3.99	2.6298×10^{-5}	2.91	1.2761×10^{-7}	3.99	1.0597×10^{-4}	2.91	8.2908×10^{-7}	3.99	2.8336×10^{-4}	2.95
64	2.1961×10^{-9}	3.98	3.4021×10^{-6}	2.95	8.0587×10^{-9}	3.99	1.3704×10^{-5}	2.91	5.2028×10^{-8}	3.99	3.6162×10^{-5}	2.97

References

[1] P. Tackley, Dynamics and evolution of the deep mantle resulting from thermal, chemical, phase and melting effects, Earth-Science Reviews 110 (2012) 1–25.

[2] M. Jacobs, A. van den Berg, Complex phase distribution and seismic velocity structure of the transition zone: Convection model predictions for a magnesium-endmember olivinepyroxene mantle, Phys. Earth. Planet. Inter. 186 (2011) 36–48.

[3] G. Jarvis, Effects of curvature on two-dimensional models of mantle convection: cylindrical polar coordinates, J. Geophys. Res. 98 (B3) (1993) 4477–4485.

[4] J. Brandenburg, E. Hauri, P. van Keken, C. Ballentine, A multiple-system study of the geochemical evolution of the mantle with force-balanced plates and thermochemical effects, Earth Planet. Sci. Lett. 276 (2008) 1–13.

[5] J. Brandenburg, P. van Keken, Methods for thermochemical convection in Earths mantle with force-balanced plates, Geochem. Geophys. Geosyst. 8 (11).

[6] I. Dione, C. Tibirna, J. Urquiza, Stokes equations with penalised slip boundary conditions, International Journal of Computational Fluid Dynamics 27 (6-7) (2013) 283–296.

[7] J. de Vries, A. van den Berg, W. van Westrenen, Formation and evolution of a lunar core from ilmenite-rich magma ocean cumulates, Earth Planet. Sci. Lett. 292 (2010) 139–147.

[8] N. Tosi, D. Yuen, Bent-shaped plumes and horizontal channel flow beneath the 660 km discontinuity, Earth Planet. Sci. Lett. 312 (2011) 348–359.

[9] J. Hernlund, P. Tackley, Modeling mantle convection in the spherical annulus, Phys. Earth. Planet. Inter. 171 (2008) 48–54.

[10] C. Hüttig, N. tosi, W. Moore, An improved formulation of the incompressible NavierStokes equations with variable viscosity, Phys. Earth. Planet. Inter. 220 (2013) 11–18.

[11] P. Arrial, N. Flyer, G. Wright, L. Kellogg, On the sensitivity of 3-D thermal convection codes to numerical discretization: a model intercomparison, Geosci. Model Dev. 7 (2014) 2065–2076.

[12] S. Zhong, A. McNamara, E. Tan, L. Moresi, M. Gurnis, A benchmark study on mantle convection in a 3-D spherical shell using CITCOMS, Geochem. Geophys. Geosyst. 9 (10).

[13] S. Zhong, M. Zuber, L. Moresi, M. Gurnis, The role of temperature-dependent viscosity and surface plates in spherical shell models of mantle convection, J. Geophys. Res. 105 (B5) (2000) 11,063–11,082.

[14] C. Burstedde, G. Stadler, L. Alisic, L. Wilcox, E. Tan, M. Gurnis, O. Ghattas, Large-scale adaptive mantle convection simulation, Geophy. J. Int. 192 (2013) 889–906.

[15] D. Davies, J. Davies, P. Bollada, O. Hassan, K. Morgan, P. Nithiarasu, A hierarchical mesh refinement technique for global 3-D spherical mantle convection modelling, Geosci. Model Dev. 6 (2013) 1095–1107.

[16] H. van Heck, J. Davies, T. Elliott, D. Porcelli, Global-scale modelling of melting and isotopic evolution of Earths mantle: melting modules for TERRA, Geosci. Model Dev. 9 (2016) 1399–1411.

[17] C. Thieulot, Analytical solution for viscous incompressible stokes flow in a spherical shell, Solid Earth Discussions 2017 (2017) 1–19. doi:10.5194/se-2017-71.
URL https://www.solid-earth-discuss.net/se-2017-71/

[18] B. Blankenbach, F. Busse, U. Christensen, L. Cserepes, D. Gunkel, U. Hansen, H. Harder, G. Jarvis, M. Koch, G. Marquart, D. Moore, P. Olson, H. Schmeling, T. Schnaubelt, A benchmark comparison for mantle convection codes, Geophys. J. Int. 98 (1989) 23–38.

[19] S. Zhong, Analytic solutions for Stokes flow with lateral variations in viscosity, Geophys. J. Int. 124 (1996) 18–28.

[20] T. Gerya, D. Yuen, Robust characteristics method for modelling multiphase visco-elasto-plastic thermo-mechanical problems, Phys. Earth. Planet. Inter. 163 (2007) 83–105.

[21] N. Tosi, C. Stein, L. Noack, C. Huettig, P. Maierova, H. Samuel, D. Davies, C. Wilson, S. Kramer, C. Thieulot, A. Glerum, M. Fraters, W. Spakman, A. Rozel, P. Tackley, A community benchmark for viscoplastic thermal convection in a 2-D square box, Geochem. Geophys. Geosyst. 16 (7) (2015) 21752196.

[22] S. Buiter, G. Schreurs, M. Albertz, T. Gerya, B. Kaus, W. Landry, L. le Pourhiet, Y. Mishin, D. Egholm, M. Cooke, B. Maillot, C. Thieulot, T. Crook, D. May, P. Souloumiac, C. Beaumont, Benchmarking numerical models of brittle thrust wedges, Journal of Structural Geology 92 (2016) 140–177.

[23] G. Schubert, D. Turcotte, P. Olson, Mantle Convection in the Earth and Planets, Cambridge University Press, 2001.

[24] W. A. Strauss, Partial Differential Equations; An Introduction, 2nd Edition, John Wiley and Sons, Hoboken, NJ, 2008.

[25] P. van Keken, S. King, H. Schmeling, U. Christensen, D. Neumeister, M.-P. Doin, A comparison of methods for the modeling of thermochemical convection, J. Geophys. Res. 102 (B10) (1997) 22,477–22,495.

[26] A. Lavecchia, C. Thieulot, F. Beekman, S. Cloetingh, S. Clark, Lithosphere erosion and continental breakup: Interaction of extension, plume upwelling and melting, Earth Planet. Sci. Lett. 467 (2017) 89–98.

[27] A. Plunder, C. Thieulot, D. van Hinsbergen, The effect of obliquity on temperature in subduction zones: insights from 3D numerical modeling, Solid Earthdoi:https://doi.org/10.5194/se-2017-134.

[28] C. Thieulot, FANTOM: two- and three-dimensional numerical modelling of creeping flows for the solution of geological problems, Phys. Earth. Planet. Inter. 188 (2011) 47–68.

[29] M. Kronbichler, T. Heister, W. Bangerth, High accuracy mantle convection simulation through modern numerical methods , Geophy. J. Int. 191 (2012) 12–29.

[30] J. Dannberg, T. Heister, Compressible magma/mantle dynamics: 3-D, adaptive simulations in ASPECT, Geophy. J. Int. 207 (2016) 1343–1366.

[31] T. Heister, J. Dannberg, R. Gassmöller, W. Bangerth, High Accuracy Mantle Convection Simulation through Modern Numerical Methods. II: Realistic Models and Problems, Geophy. J. Int. 210 (2) (2017) 833–851.

[32] W. Bangerth, R. Hartmann, G. Kanschat, deal.II - a general purpose object oriented finite element library, ACM Transaction on mathematical software 33 (4).

[33] M. H. et al, An overview of the Trilinos project, ACM Trans. Math. Softw. 31 (2005) 397–423.

[34] C. Burstedde, L. C. Wilcox, O. Ghattas, `p4est`: Scalable algorithms for parallel adaptive mesh refinement on forests of octrees, SIAM Journal on Scientific Computing 33 (3) (2011) 1103–1133. doi:10.1137/100791634.

[35] W. Bangerth, J. Dannberg, R. Gassmöller, T. Heister, et al., ASPECT: Advanced Solver for Problems in Earth's ConvecTion, User ManualDoi:10.6084/m9.figshare.4865333. doi:10.6084/m9.figshare.4865333.
URL https://doi.org/10.6084/m9.figshare.4865333

[36] M. Thielmann, D. May, B. Kaus, Discretization errors in the Hybrid Finite Element Particle-In-Cell Method, Pure and Applied Geophysics.